Radiolabeled Monoclonal Antibodies Specific to the Extracellular Domain of Prostate-Specific Membrane Antigen: Preclinical Studies in Nude Mice Bearing LNCaP Human Prostate Tumor

Peter M. Smith-Jones, PhD[1]; Shankar Vallabhajosula, PhD[1]; Vincent Navarro, MS[2]; Diego Bastidas, MS[1]; Stanley J. Goldsmith, MD[1]; and Neil H. Bander, MD[2]

[1]Division of Nuclear Medicine, Department of Radiology, New York Presbyterian Hospital–Weill Medical College of Cornell University, New York, New York; and [2]Laboratory of Urological Oncology, Department of Urology, New York Presbyterian Hospital–Weill Medical College of Cornell University, New York, New York

Prostate-specific membrane antigen (PSMA), a transmembrane glycoprotein, is highly expressed by virtually all prostate cancers. PSMA is also expressed on the tumor vascular endothelium of virtually all solid carcinomas and sarcomas but not on normal vascular endothelium. PSMA is currently the focus of several diagnostic and therapeutic strategies. We have previously reported on the radiolabeling and in vitro binding properties of monoclonal antibodies (mAbs) (J415, J533, and J591) that recognize and bind with high affinity to the extracellular domain of PSMA ($PSMA_{ext}$). This article reports on the in vivo behavior and tumor uptake of ^{131}I- and ^{111}In-labeled anti-$PSMA_{ext}$ mAbs (J415, J533, and J591) and their potential utility for radioimmunotherapy. **Methods:** In nude mice bearing PSMA-positive human LNCaP tumors, the pharmacokinetics, biodistribution, and tumor uptake of these antibodies was compared with ^{111}In-7E11 mAb, specific to the intracellular domain of PSMA ($PSMA_{int}$). Autoradiographic studies were done to identify intratumoral distribution of radiolabeled mAbs. **Results:** With ^{131}I-labeled antibodies, the net tumor retention of radioactivity by day 6 was significantly higher with J415 (15.4% ± 1.1%) and 7E11 (14.5% ± 1.7%) than with J591 (9.58% ± 1.1%). By contrast, the tumor uptake of ^{111}In-1,4,7,10-tetraazacyclododecane-N,N′,N″,N‴-tetraacetic acid–labeled J415 and J591 gradually increased with time and was quite similar to that of 7E11. In addition, the blood clearance of ^{111}In-labeled J415 and J591 antibodies was relatively faster than that of radiolabeled 7E11. As a consequence, the tumor-to-blood ratios with J415 and J591 were higher than that of 7E11. The localization of radiolabeled anti-$PSMA_{ext}$ antibodies in PSMA-positive LNCaP tumors was highly specific because the tumor uptake of ^{131}I-labeled J415 and J591 was more than twice that of a nonspecific antibody. Furthermore, the tumor uptake of ^{131}I-J591 was almost 20 times higher in PSMA-positive LNCaP tumors than in PSMA-negative PC3 and DU145 tumor xenografts. Autoradiographic studies suggested that 7E11 (anti-$PSMA_{int}$) distinctly favors localization to areas of necrosis whereas J415 and J591 (anti-$PSMA_{ext}$) demonstrated a distinct preferential accumulation in areas of viable tumor. **Conclusion:** These results clearly demonstrate that PSMA-specific internalizing antibodies such as J415 and J591 may be the ideal mAbs for the development of novel therapeutic methods to target the delivery of β-emitting radionuclides (^{131}I, ^{90}Y, and ^{177}Lu) for the treatment of PSMA-positive tumors. In addition, because J591 and J415 mAbs are specific to $PSMA_{ext}$, thus targeting viable tumor, these immunoconjugates are better candidates for targeted radioimmunotherapy than are antibodies targeting $PSMA_{int}$.

Key Words: monoclonal antibody; prostate-specific membrane antigen; ^{131}I-huJ591; ^{111}In-DOTA-huJ591; tumor localization

J Nucl Med 2003; 44:610–617

Various studies have shown that prostate-specific membrane antigen (PSMA), a 100-kDa type II transmembrane glycoprotein, is highly expressed by virtually all prostate cancers (*1–3*). In contrast to other highly restricted prostate-related antigens such as prostate-specific antigen, prostate secretory protein, and prostatic acid phosphatase, which are secretory proteins, PSMA is an integral membrane protein and is not appreciably released into the circulation (*4*). In healthy subjects, PSMA expression is highly prostate specific (*5*) and its expression has been shown to be upregulated in poorly differentiated (*4*) and advanced prostate cancer (*1*) as well as after androgen-deprivation therapy (*6*). PSMA is also expressed on the tumor vascular endothelium of virtually all solid carcinomas and sarcomas (*1,5–10*) but not on normal vascular endothelium, making it potentially useful as an antibody-mediated diagnostic and therapeutic target across a wide spectrum of solid tumors. PSMA is currently the focus of several diagnostic and therapeutic strategies (*11–13*).

PSMA was initially identified using the 7E11/CYT 356 monoclonal antibody (mAb) (*14*), which binds to an intra-

Received Jul. 9, 2002; revision accepted Nov. 14, 2002.

For correspondence or reprints contact: Shankar Vallabhajosula, PhD, 525 E. 68th St., STARR-221, Weill Medical College of Cornell University, New York, NY 10021.

E-mail: svallabh@med.cornell.edu

cellular epitope of PSMA ($PSMA_{int}$) (*15*). ^{111}In-labeled 7E11 mAb (capromab pendetide, or ProstaScint; Cytogen Corp., Princeton, NJ) has been approved by the Food and Drug Administration for diagnostic imaging of prostate cancer in lymph nodes or the prostate bed (*16,17*). Radiolabeled 7E11 antibody does not bind to viable cells but only to $PSMA_{int}$, which may be accessible only in dead, dying, or apoptotic cells within tumor sites. To target viable tumor cells, we and others have developed mAbs specific to the extracellular domain of PSMA ($PSMA_{ext}$) (*7,13*).

In 1997, we reported the development of 4 IgG mAbs that react with $PSMA_{ext}$ and defined 2 distinct epitopes of PSMA (*7,18*). Recently, we reported on the radiolabeling and in vitro binding properties of 3 of these mAbs (J415, J533, and J591), which recognize and bind with high affinity to $PSMA_{ext}$ (*19*). To label mAbs with ^{111}In, the antibody was first conjugated with 5 molecules of 1,4,7,10-tetraazacyclododecane-N,N′,N″,N‴-tetraacetic acid (DOTA), a macrocyclic chelating agent. Saturation binding studies demonstrated that both ^{131}I- and ^{111}In-labeled J415 and J591 bind to PSMA-positive LNCaP cells with high affinity whereas J533 binds to cells with lower affinity. By contrast, radiolabeled 7E11 bound to fewer sites expressed by intact LNCaP cells (i.e., the exposed $PSMA_{ext}$). With J591 and J415, ^{111}In activity was retained within the cell whereas the ^{131}I activity rapidly diffused out of the cell, probably because of dehalogenation. The in vitro studies clearly demonstrated that radiolabeled J415 and J591 mAbs are ideal radiopharmaceuticals for targeting viable PSMA-positive tumors.

This article reports the in vivo behavior of the ^{111}In- and ^{131}I-labeled mAbs (J591, J415, and J533) specific to $PSMA_{ext}$. In nude mice bearing LNCaP tumors, the pharmacokinetics, biodistribution, and tumor uptake of these antibodies were compared with those of radiolabeled 7E11. Control studies with radiolabeled irrelevant antibodies and nude mice bearing PSMA-negative tumors were also performed to investigate the specificity of radiolabeled J591 and J415.

MATERIALS AND METHODS

All reagents were obtained from commercial sources. ^{111}In and ^{131}I were purchased from Nordion (Kanata, Ontario). To reduce metallic contamination, all reagents used to modify and purify the mAbs were made with deionized water. Ammonium acetate buffer and sodium phosphate buffer were also purified with Chelex 100 (Bio-Rad, Richmond, CA) to remove any metal ions. Murine mAbs J415, J533, and J591 were prepared as described earlier (*7*). Purified 7E11 was generously provided by Gerald P. Murphy (Pacific Northwest Research Foundation, Seattle, WA). Diethylenetriaminepentaacetic acid (DTPA)-7E11 (capromab pendetide) was purchased from Cytogen Corp.

Radiolabeled mAbs

The mAbs J415, J533, J591, and 7E11 and an irrelevant IgG (anti-CD20) were labeled with ^{131}I using the IODO-GEN method (Pierce Biotechnology, Inc., Rockford, IL) (*20*) to a specific activity of 400 MBq/mg (*19,21*). For ^{111}In labeling, the J415 and J591 antibodies were first conjugated with DOTA, by direct coupling of 1 of the 4 carboxylic acid groups of DOTA to the primary amines in the antibody protein structure (*19*). These conjugates were labeled with ^{111}In to produce specific activities of 200 MBq/mg. DTPA-7E11/CYT-356 (ProstaScint) was radiolabeled with ^{111}In according to the manufacturer's procedure. Before injection into mice, the radiolabeled antibody preparations were filtered using a 0.22-μm membrane filter and diluted in phosphate-buffered saline (pH 7.4, 0.2% bovine serum albumin). Radiolabeled antibodies were also assayed for immunoreactivity by the method of Lindmo et al. (*19,22*).

Biodistribution Studies

Prostate carcinoma cell lines LNCaP, DU145, and PC3 (American Type Culture Collection, Rockville, MD) were grown in RPMI 1640, supplemented with 10% fetal calf serum, at a temperature of 37°C in an environment containing 5% CO_2. Before use, the cells were trypsinized, counted, and suspended in Matrigel (Collaborative Biomedical Products, Bedford, MA). Nu/Nu BALB/c mice 8–10 wk old were inoculated, in the right and left flanks, with a 0.1-mL cell suspension containing 5×10^6 LNCaP cells. After 14–18 d, tumors (100–300 mg) had developed. The PSMA-negative DU145 and PC3 cells were implanted in nude mice in an identical manner.

The tumor-bearing mice received an injection through the tail vein of 0.2 mL of ^{131}I- or ^{111}In-labeled mAb preparation in a 0.2-mL volume containing about 80 kBq of radioactivity. Groups of animals (3–8 per group) were sacrificed after 2, 4, or 6 d. The major organs and tumors were recovered. Blood samples were also obtained at the time of sacrifice. The blood and tissue samples were weighed and counted with appropriate standards in an automatic NaI(Tl) counter. The background-corrected relative activity (cpm) of tissue samples was expressed as a percentage of the injected dose per gram (%ID/g). The blood time–activity curves were fitted with a monoexponential least squares regression analysis (Origin; Microcal, Northampton, MA) to determine the rate of clearance of radiolabeled antibodies from circulation.

To demonstrate tumor localization by imaging studies, 2 MBq of ^{111}In-DOTA-J591 were injected into the tumor-bearing mice ($n = 4$). On days 1–4 and 6 after injection, the mice were sedated with ketamine, 100 mg/kg, and xylazine, 10 mg/kg, administered intraperitoneally. The images of mice were obtained with a gamma camera (Transcam; ADAC Laboratories, Milpitas, CA) fitted with a pinhole collimator in a 256×256 matrix for 1,000 s using the 245-keV photopeak of ^{111}In with a 20% window.

Autoradiography

For several animals ($n = 20$), harvested tumor samples were immediately cooled in liquid nitrogen and frozen in embedding medium (O.C.T. 4583; Sakura Finetec, Torrance CA). Twenty-micrometer sections were cut, and the tumor sections were either fixed with acetone and placed in direct contact with a sheet of photographic film (Biomax; Kodak, Rochester, NY) for 12–14 d or stained with hematoxylin and eosin (H and E) before exposure of the film. For ex vivo autoradiography studies, tumors from untreated control animals were collected and cut into 10-μm sections. These sections were soaked in Tris buffer (170 mmol/L, pH 7.4, with 2 mmol/L $CaCl_2$ and 5 mmol/L KCl) for 15 min, washed with the same buffer, and incubated with ^{131}I-J591 mAb (5 kBq) for 1 h at 4°C. Nonspecific binding was determined in the presence of 100 nmol/L J591 mAb. These sections were then washed 3 times with

phosphate-buffered saline (containing 0.2% bovine serum albumin) and once with Tris buffer before being fixed with acetone and then exposed to photographic film.

RESULTS

Biodistribution of ^{131}I-Labeled mAbs

In nude mice bearing LNCaP tumors, the biodistribution and tumor uptake of ^{131}I-labeled J415, J533, and J591 were compared with those of ^{131}I-7E11. At 2 d after injection (Table 1), J415, J591, and 7E11 had similar tumor uptake and blood-pool activity. On days 4 and 6, there were significant differences among these 3 antibodies (Tables 2 and 3). On day 6, the tumor uptake (%ID/g) of both J415 (15.4 ± 1.1) and 7E11 (14.5 ± 1.7) was similar and significantly higher than that of J591 (9.58 ± 1.1). The blood activity of both J415 and J591 was significantly lower than that of 7E11. With the ^{131}I-labeled mAbs, the tumor-to-blood and tumor-to-muscle ratios were higher with J415 than with J591 or with 7E11 (Figs. 1A and 1C). Among the 3 mAbs specific to $PSMA_{ext}$, ^{131}I-J533 had a significantly lower tumor uptake and a higher blood-pool activity than did J415 or J591. As a result, the tumor-to-blood and tumor-to-muscle ratios were significantly lower with J533 (Tables 1 and 2).

To assess the specificity of radiolabeled mAb localization in PSMA-positive LNCaP tumors, the uptake of ^{131}I-labeled J415 and J591 in selected organs was compared with that of an irrelevant IgG antibody (Table 4). At 1 d after injection, the tumor uptake (%ID/g) of both J415 (12.2 ± 3.24) and J591 (8.55 ± 1.29) was significantly higher than that of an irrelevant antibody (4.41 ± 0.40). Liver uptake of J415 and J591 was also significantly higher than liver uptake of the irrelevant nonspecific antibody. Uptake in other organs (lung, kidney, and muscle) was similar with all 3 antibodies. In a second control study, tumor uptake of ^{131}I-J591 was determined in nude mice bearing the PSMA-negative prostate tumors (PC3 and DU145). At 4 d after injection, tumor uptake of J591 was only 0.66 ± 0.07 in PC3 tumors (n = 10) and 0.55 ± 0.03 in DU145 tumors (n = 6). In contrast, tumor uptake of ^{131}I-J591 (11.4 ± 1.49) in PSMA-positive LNCaP tumors (Table 2) was significantly greater than in PSMA-negative tumors ($P < 0.01$).

Biodistribution of ^{111}In-Labeled mAbs

With ^{111}In, tumor uptake of J415 and J591 gradually increased with time and was quite similar to that of 7E11 (Tables 1–3). However, blood clearance of ^{111}In-labeled J415 and J591 antibodies was relatively faster than that of 7E11. At 6 d after injection, the blood activity of J415 (2.63 ± 0.23) and J591 (2.52 ± 0.16) was about 40% less than that with 7E11 (4.16 ± 0.21). As a consequence, the tumor-to-blood ratios with J415 and J591 were higher than that with 7E11 (Fig. 1B). There were minor differences in the uptake of these 3 antibodies in liver, spleen, and kidney. The ^{131}I mAb tumor uptake was systematically lower than tumor uptake of the corresponding ^{111}In-labeled mAbs and probably reflected internalization of the mAbs and their cellular metabolism. Consequently, the highest tumor-to-blood ratios were obtained with the^{111}In-labeled J415 and J591 at 6 d after injection.

The serial gamma camera images (Fig. 2) of a nude mouse clearly show the intense tumor accumulation of

TABLE 1
Biodistribution of Radiolabeled mAbs and Tumor-to-Nontumor Organ Ratios in Nude Mice Bearing LNCaP Tumors at 2 Days After Injection

Organ	^{131}I-J415 (n = 8)	^{131}I-J533 (n = 4)	^{131}I-J591 (n = 8)	^{131}I-7E11 (n = 7)	^{111}In-J415 (n = 4)	^{111}In-J591 (n = 4)	^{111}In-7E11 (n = 4)
Blood	8.44 ± 2.16[a]	12.80 ± 1.1[ad]	8.57 ± 2.04[d]	10.80 ± 3.5	6.12 ± 0.62[gh]	8.98 ± 2.10[g]	7.22 ± 0.46[h]
Heart	2.71 ± 0.66[ac]	4.82 ± 1.47[ad]	2.78 ± 0.62[df]	3.92 ± 0.99[cf]	2.87 ± 0.44	3.10 ± 0.36	2.72 ± 0.81
Lung	4.38 ± 0.92	5.08 ± 0.45	4.65 ± 1.77	4.68 ± 0.54	4.15 ± 0.99[gh]	5.89 ± 0.30[gi]	4.64 ± 0.27[hi]
Liver	2.56 ± 0.63[a]	3.78 ± 0.50[ade]	2.71 ± 0.50[d]	2.96 ± 0.52[e]	5.18 ± 1.07[gh]	7.68 ± 0.50[gi]	4.49 ± 0.51[hi]
Kidney	2.05 ± 0.41[b]	3.37 ± 0.39[de]	2.11 ± 0.57[bd]	2.16 ± 0.88[e]	4.21 ± 0.07[gh]	5.25 ± 0.63[gi]	2.55 ± 0.27[hi]
Stomach	1.37 ± 0.37	1.11 ± 0.34	1.46 ± 0.40	1.17 ± 0.26	1.16 ± 0.29	0.73 ± 0.18	0.92 ± 0.37
Small intestine	1.01 ± 0.37	0.84 ± 0.07	0.86 ± 0.18	0.94 ± 0.09	1.39 ± 0.06	1.32 ± 0.26[i]	1.06 ± 0.19[i]
Large intestine	0.50 ± 0.21	0.43 ± 0.13	0.54 ± 0.13[f]	0.39 ± 0.06[f]	0.76 ± 0.13[g]	0.98 ± 0.06[g]	0.70 ± 0.13
Muscle	0.70 ± 0.19[a]	1.13 ± 0.26[ad]	0.62 ± 0.19[df]	0.95 ± 0.24[f]	0.83 ± 0.09	0.67 ± 0.10	0.83 ± 0.37
Thyroid	18.90 ± 5.9[a]	30.20 ± 8.3[ade]	15.70 ± 10.57[df]	19.4 ± 4.1[ef]	2.19 ± 0.72	2.47 ± 0.37[i]	1.67 ± 0.19[i]
Spleen	2.47 ± 0.62	2.60 ± 0.29	2.88 ± 0.89	2.40 ± 0.45	4.48 ± 1.11	5.36 ± 1.25	3.94 ± 1.13
Tumor	13.00 ± 5.1	7.38 ± 0.97[d]	11.20 ± 2.9[d]	11.70 ± 4.3	11.3 ± 1.0[h]	13.6 ± 2.8[i]	9.3 ± 1.52[hi]
Tumor/blood	1.57 ± 0.42[ac]	0.58 ± 0.04[ade]	1.43 ± 0.57[d]	1.08 ± 0.18[ce]	1.83 ± 0.33	1.62 ± 0.72	1.34 ± 0.24
Tumor/liver	5.19 ± 1.35[a]	1.96 ± 0.18[ade]	4.37 ± 1.15[d]	3.89 ± 0.92[e]	2.20 ± 0.52	1.76 ± 0.22	2.16 ± 0.44
Tumor/spleen	5.45 ± 1.69[a]	2.84 ± 0.32[a]	3.85 ± 1.55	3.73 ± 1.55	2.59 ± 0.76	2.39 ± 0.86	2.59 ± 0.92
Tumor/muscle	19.20 ± 6.0[ac]	6.80 ± 1.56[ade]	20.0 ± 6.9[df]	12.3 ± 2.2[cef]	13.4 ± 1.4	21.10 ± 7.4	13.80 ± 7.8

Data are %ID/g, expressed as mean ± SD. Difference between means in following groups is significant ($P < 0.05$): (a) ^{131}I-J415 vs. ^{131}I-J533; (b) ^{131}I-J415 vs. ^{131}I-J591; (c) ^{131}I-J415 vs. ^{131}I-7E11; (d) ^{131}I-J533 vs. ^{131}I-J519; (e) ^{131}I-J533 vs. ^{131}I-7E11; (f) ^{131}I-J591 vs. ^{131}I-7E11; (g) ^{111}In-J415 vs. ^{111}In-J519; (h) ^{111}In-J415 vs. ^{111}In-7E11; (i) ^{111}In-J591 vs. ^{111}In-7E11.

TABLE 2
Biodistribution of Radiolabeled MAbs and Tumor-to-Nontumor Organ Ratios in Nude Mice Bearing LNCaP Tumors at 4 Days After Injection

Organ	^{131}I-J415 (n = 9)	^{131}I-J533 (n = 4)	^{131}I-J591 (n = 7)	^{131}I-7E11 (n = 8)	^{111}In-J415 (n = 4)	^{111}In-J591 (n = 7)	^{111}In-7E11 (n = 4)
Blood	6.11 ± 0.97[ac]	10.3 ± 0.48[ade]	5.96 ± 1.61[d]	7.72 ± 1.79[ce]	4.42 ± 0.78	4.78 ± 0.85	5.69 ± 1.00
Heart	2.01 ± 0.54[a]	2.87 ± 0.71[ad]	1.70 ± 0.16[fd]	2.59 ± 1.03	1.84 ± 0.45	1.82 ± 0.37	1.58 ± 0.49
Lung	3.51 ± 0.85	4.49 ± 1.05	3.35 ± 0.97	3.80 ± 0.76	3.72 ± 0.50	3.40 ± 0.32	4.03 ± 1.03
Liver	1.97 ± 0.40[a]	2.56 ± 0.18[ae]	2.06 ± 0.46	1.93 ± 0.33[e]	5.47 ± 0.50[h]	7.66 ± 2.44[i]	4.39 ± 0.45[hi]
Kidney	1.94 ± 0.60[b]	2.27 ± 0.55[de]	1.37 ± 0.24[bd]	1.66 ± 0.33[e]	5.22 ± 0.57[h]	5.39 ± 1.27	3.81 ± 2.08
Stomach	0.96 ± 0.55	0.98 ± 0.21	1.06 ± 0.36	0.96 ± 0.23	1.35 ± 0.37[g]	0.80 ± 0.15[g]	1.02 ± 0.35
Small intestine	0.62 ± 0.29	0.76 ± 0.13[d]	0.53 ± 0.13[fd]	0.77 ± 0.08	1.69 ± 0.19[gh]	1.31 ± 0.19[gi]	0.94 ± 0.06[hi]
Large intestine	0.32 ± 0.16[c]	0.31 ± 0.04[e]	0.34 ± 0.10[f]	0.48 ± 0.10[ce]	0.88 ± 0.06[h]	0.81 ± 0.20[i]	0.50 ± 0.07[hi]
Muscle	0.62 ± 0.37	0.93 ± 0.28[d]	0.48 ± 0.24[d]	0.72 ± 0.27	0.60 ± 0.03	0.55 ± 0.34	0.51 ± 0.13
Thyroid	26.6 ± 17.9	33.7 ± 6.9[e]	26.5 ± 26.2	21.3 ± 7.9[e]	1.82 ± 0.70	1.90 ± 0.16[i]	1.29 ± 0.69[i]
Spleen	2.43 ± 1.04[a]	2.33 ± 0.38[a]	2.33 ± 0.72	1.99 ± 0.69	4.63 ± 1.38	4.43 ± 0.89	3.88 ± 1.51
Tumor	17.0 ± 6.6[a]	7.29 ± 2.5	11.4 ± 4.21	12.1 ± 5.3	16.7 ± 2.6	15.7 ± 3.5	16.2 ± 4.29
Tumor/blood	2.80 ± 0.70[ac]	0.72 ± 0.29[ad]	2.14 ± 0.53[d]	1.58 ± 0.79[c]	3.17 ± 0.37	3.35 ± 0.39	2.83 ± 0.51
Tumor/liver	9.07 ± 3.19[a]	2.81 ± 0.85[ad]	6.41 ± 2.89[d]	6.32 ± 3.41	2.32 ± 0.16	2.19 ± 0.47[i]	3.71 ± 1.11[i]
Tumor/spleen	7.70 ± 3.81[a]	3.06 ± 0.65[ade]	5.71 ± 2.21[d]	5.91 ± 1.67[e]	2.50 ± 0.11[gh]	3.67 ± 0.71[g]	4.32 ± 0.85[h]
Tumor/muscle	30.7 ± 11.3[ac]	7.85 ± 1.25[ade]	29.9 ± 10.3[df]	18.1 ± 8.0[ce]	21.8 ± 2.4[h]	40.1 ± 22.6	32.1 ± 4.9[h]

Data are %ID/g, expressed as mean ± SD. Difference between means in following groups is significant ($P < 0.05$): (a) ^{131}I-J415 vs. ^{131}I-J533; (b) ^{131}I-J415 vs. ^{131}I-J591; (c) ^{131}I-J415 vs. ^{131}I-7E11; (d) ^{131}I-J533 vs. ^{131}I-J519; (e) ^{131}I-J533 vs. ^{131}I-7E11; (f) ^{131}I-J591 vs. ^{131}I-7E11; (g) ^{111}In-J415 vs. ^{111}In-J519; (h) ^{111}In-J415 vs. ^{111}In-7E11; (i) ^{111}In-J591 vs. ^{111}In-7E11.

^{111}In-DOTA-J591. On day 1, the single tumor (approximately 250 mg) on the right hindquarter, the blood pool, and the liver were well visualized. But in the later images, although the activity had cleared from the blood pool, the tumor accumulation became gradually more intense, compared with liver activity.

Autoradiography

Tumor specimens were harvested for staining with H and E and autoradiography to study the intratumoral biodistribution of ^{131}I-labeled mAbs 4–6 d after intravenous injection. The H and E staining revealed a considerable amount of necrosis, averaging 50% of the cross-sectional area, in all

TABLE 3
Biodistribution of Radiolabeled MAbs and Tumor-to-Nontumor Organ Ratios in Nude Mice Bearing LNCaP Tumors at 6 Days After Injection

Organ	^{131}I-J415 (n = 5)	^{131}I-J591 (n = 8)	^{131}I-7E11 (n = 8)	^{111}In-J415 (n = 4)	^{111}In-J591 (n = 8)	^{111}In-7E11 (n = 4)
Blood	3.95 ± 0.99[b]	4.42 ± 1.74[c]	7.13 ± 1.90[bc]	2.63 ± 0.47[e]	2.52 ± 0.56[f]	4.16 ± 0.41[ef]
Heart	1.57 ± 0.47[b]	1.42 ± 0.60[c]	2.46 ± 0.46[bc]	1.30 ± 0.10	1.28 ± 0.24	2.42 ± 1.49
Lung	2.61 ± 1.00	2.29 ± 0.91[c]	3.52 ± 0.59[c]	3.07 ± 0.67	2.47 ± 0.65	3.20 ± 0.16
Liver	1.74 ± 0.91	1.31 ± 0.34[c]	2.01 ± 0.49[c]	4.69 ± 0.61[d]	6.08 ± 0.83[df]	4.37 ± 0.46[f]
Kidney	1.36 ± 0.62	1.20 ± 0.51	1.65 ± 0.39	4.67 ± 0.45[e]	4.53 ± 0.87[f]	2.85 ± 0.26[e]
Stomach	0.54 ± 0.19	0.47 ± 0.15	0.47 ± 0.23	0.44 ± 0.20	0.46 ± 0.17	0.31 ± 0.07
Small intestine	0.47 ± 0.15	0.35 ± 0.09[c]	0.52 ± 0.14[c]	0.93 ± 0.04[e]	0.84 ± 0.13[f]	0.64 ± 0.08[ef]
Large intestine	0.30 ± 0.16	0.24 ± 0.07[c]	0.38 ± 0.12[c]	0.71 ± 0.13	0.57 ± 0.10	0.64 ± 0.06
Muscle	0.30 ± 0.06[b]	0.33 ± 0.18[c]	0.74 ± 0.31[bc]	0.35 ± 0.11	0.30 ± 0.10	0.36 ± 0.08
Thyroid	28.5 ± 13.1	35.1 ± 18.4	29.3 ± 10.6	1.66 ± 0.22[de]	0.85 ± 0.36[df]	1.38 ± 0.25[ef]
Spleen	1.37 ± 0.25	1.74 ± 0.72	1.74 ± 0.38	4.32 ± 1.32	3.36 ± 0.61	3.14 ± 0.60
Tumor	15.4 ± 2.4[a]	9.58 ± 3.2[ac]	14.5 ± 4.8[c]	17.7 ± 3.1	17.4 ± 3.5	18.7 ± 2.2
Tumor/blood	4.49 ± 1.81[ab]	2.28 ± 0.77[a]	2.21 ± 1.33[b]	6.78 ± 0.78[e]	6.07 ± 1.79	4.57 ± 0.31[e]
Tumor/liver	11.7 ± 5.5	7.21 ± 1.80	7.38 ± 2.40	3.79 ± 0.47[e]	3.22 ± 0.52[f]	4.33 ± 0.85[ef]
Tumor/spleen	9.69 ± 3.73	6.90 ± 2.20	8.89 ± 3.84	4.57 ± 2.33	5.14 ± 0.95	6.52 ± 2.32
Tumor/muscle	56.1 ± 11.2[ab]	34.1 ± 15.9[a]	21.8 ± 12.9[b]	52.1 ± 11.2[d]	64.3 ± 5.9[d]	55.6 ± 12.8

Data are %ID/g, expressed as mean ± SD. Difference between means in following groups is significant ($P < 0.05$): (a) ^{131}I-J415 vs. ^{131}I-J591; (b) ^{131}I-J415 vs. ^{131}I-7E11; (c) ^{131}I-J591 vs. ^{131}I-7E11; (d) ^{111}In-J415 vs. ^{111}In-J519; (e) ^{111}In-J415 vs. ^{111}In-7E11; (f) ^{111}In-J591 vs. ^{111}In-7E11.

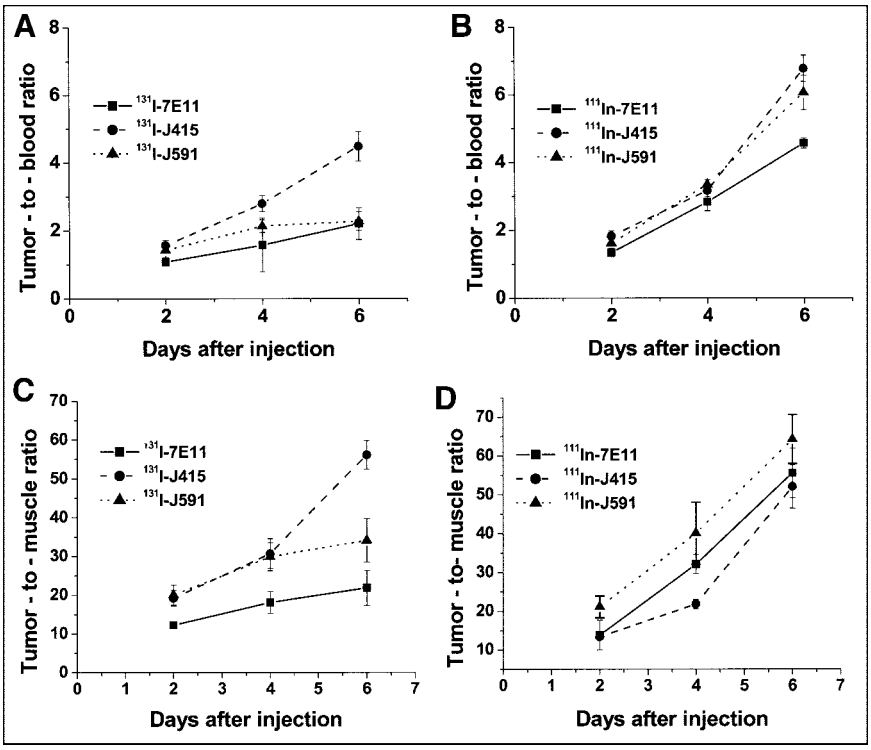

FIGURE 1. Tumor-to-blood (A and B) and tumor-to-muscle (C and D) ratios of ^{131}I- and ^{111}In-labeled anti-PSMA mAbs in nude mice with LNCaP tumors.

specimens studied (Figs. 3 and 4). The autoradiographs revealed a focal, somewhat heterogeneous distribution pattern with all 3 antibodies. Interestingly, the biodistribution pattern with mAbs to $PSMA_{int}$ and $PSMA_{ext}$ revealed almost reciprocal patterns. That is, 7E11 (anti-$PSMA_{int}$) distinctly favored localization to areas of necrosis (e.g., Fig. 3A), whereas J 591 and J415 (anti-$PSMA_{ext}$) demonstrated a distinct preferential accumulation in areas of viable tumor (Figs. 3B and 3C). Ex vivo autoradiography (Fig. 4), for which ^{131}I-J591 was incubated directly on the tissue section, demonstrated a homogeneous binding pattern.

TABLE 4
Uptake of Radiolabeled mAbs and Tumor-to-Nontumor Organ Ratios in Nude Mice Bearing LNCaP Tumors at 1 Day After Injection

Organ	^{131}I-B1 (n = 4)	^{131}I-J415 (n = 3)	^{131}I-J591 (n = 8)
Blood	10.10 ± 1.30	11.10 ± 1.9	12.90 ± 2.6
Heart	2.86 ± 0.51	3.39 ± 0.98	4.06 ± 1.07
Lung	4.30 ± 0.20	5.37 ± 1.32	5.25 ± 1.20
Liver	2.17 ± 0.28[ab]	3.31 ± 0.55[a]	4.11 ± 0.92[b]
Kidney	2.29 ± 0.28	2.83 ± 0.50	2.77 ± 0.71
Stomach	1.54 ± 0.31[b]	2.04 ± 0.40	2.82 ± 0.85[b]
Small intestine	1.15 ± 0.05	1.01 ± 0.22	1.14 ± 0.25
Large intestine	0.38 ± 0.07[b]	0.57 ± 0.03	0.93 ± 0.38[b]
Muscle	0.86 ± 0.11	0.74 ± 0.30	0.60 ± 0.52
Thyroid	16.70 ± 12.0	7.73 ± 5.31[c]	15.20 ± 1.6[c]
Spleen	—	3.36 ± 0.46	3.15 ± 0.62
Tumor	4.41 ± 0.80[a]	12.2 ± 3.24[a]	8.55 ± 3.66
Tumor/blood	0.45 ± 0.14[a]	1.11 ± 0.13[ac]	0.70 ± 0.28[c]
Tumor/muscle	5.15 ± 0.70[ab]	18.8 ± 8.2[a]	10.60 ± 6.0[b]
Tumor/liver	2.08 ± 0.54[a]	3.73 ± 0.58[a]	2.27 ± 1.23
Tumor/spleen	—	3.67 ± 0.61[c]	2.45 ± 0.40[c]

Data are %ID/g, expressed as mean ± SD. Difference between means in following groups is significant ($P < 0.05$): (a) ^{131}I-B1 vs. ^{131}I-J415; (b) ^{131}I-B1 vs. ^{131}I-J591; (c) ^{131}I-J415 vs. ^{131}I-J591.

DISCUSSION

On the basis of in vitro studies, we previously reported that mAbs specific to $PSMA_{ext}$ are ideal agents to develop radiopharmaceuticals for targeting viable PSMA-positive tumors (*19*). This study examined the in vivo behavior and tumor uptake of ^{131}I- and ^{111}In-labeled mAbs (J591, J415, and J533) specific to $PSMA_{ext}$. In addition, the pharmacokinetics, biodistribution, and tumor uptake of these radiola-

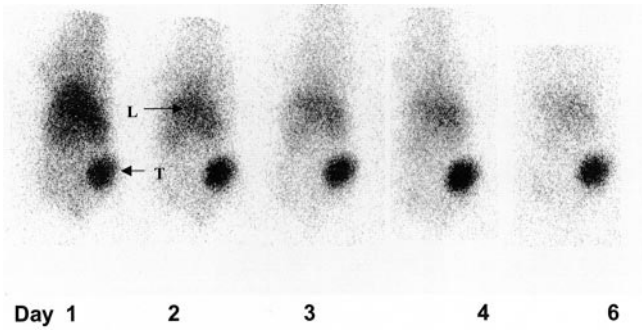

FIGURE 2. Tumor localization of ^{111}In-DOTA-J591 in nude mouse bearing LNCaP tumor (250 mg). Gamma camera images of same mouse were obtained on different days. L = liver; T = tumor.

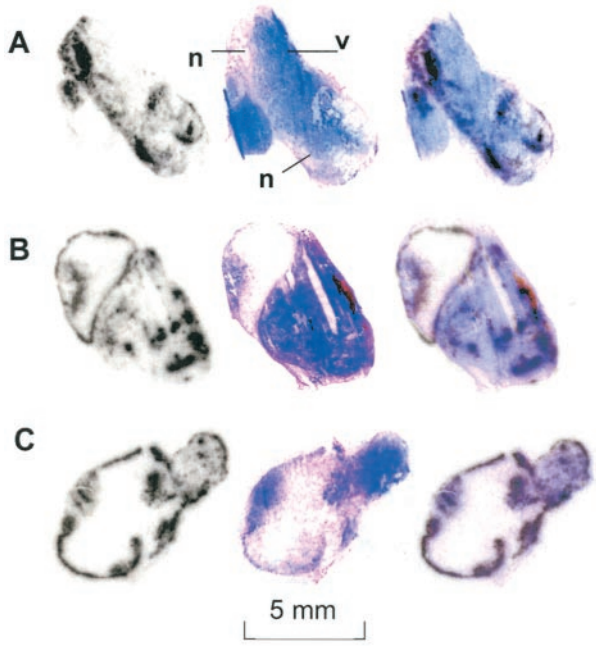

FIGURE 3. Autoradiographs and H- and E-stained sections of LNCaP xenografts harvested 4–6 d after intravenous injection of ^{131}I-labeled 7E11 (A), J591 (B), and J415 (C). Column 1 = autoradiograph; column 2 = stained section; column 3 = composite image of autoradiograph and stained section. Considerable areas of necrosis were evident in all tumors. Focality of mAb localization is evident on autoradiograph. Also evident is preferential uptake of 7E11 to areas of necrosis (n) and J415 and J591 to areas of viable tumor (v).

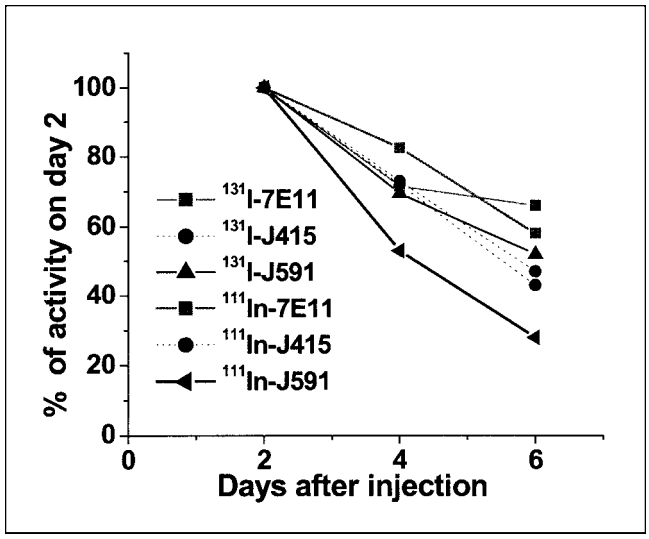

FIGURE 5. Blood clearance of radiolabeled antibodies as function of time. For each radiolabeled antibody, %ID/g on days 4 and 6 was normalized to value on day 2. ^{111}In-labeled J591 has faster blood clearance than radiolabeled 7E11.

beled mAbs were compared with those of radiolabeled 7E11, which is specific to the $PSMA_{int}$.

In nude mice with PSMA-positive LNCaP tumors, the tumor uptake of ^{131}I-labeled J415 and J591 is more than twice that of an irrelevant antibody whereas the blood-pool activity is similar for both specific and nonspecific antibodies (Table 4). The biodistribution and tumor uptake of an irrelevant antibody may be due to both organ perfusion and nonspecific accumulation. In addition, we have also demonstrated that tumor uptake of ^{131}I-J591 is almost 20 times higher in PSMA-positive LNCaP tumors than in PSMA-negative PC3 and DU145 tumor xenografts. Interestingly, with mAb 7E11 specific for $PSMA_{int}$, it was reported (*23*) that at 4 d after injection, tumor uptake of ^{111}In-DTPA-7E11 in PSMA-positive LNCaP tumors (16.7 ± 1.3 %ID/g) was only 3 times higher than that in PSMA-negative tumors DU145 (5.1 %ID/g) and PC3 (5.1 %ID/g).

Among the 3 mAbs specific to $PSMA_{ext,}$ ^{131}I-J533 showed significantly lower tumor localization than either J415 or J591 (Tables 1 and 2). In addition, both the tumor-to-blood and the tumor-to-muscle ratios were significantly reduced, compared with J415 and J591. This finding is consistent with our previous in vitro saturation binding studies (*19*), which clearly demonstrated that J533 had a significantly lower affinity to PSMA (dissociation constant [K_d] = 18 ± 5 nmol/L) than did J415 (K_d = 1.76 ± 0.69 nmol/L) or J591 (K_d = 1.83 ± 1.21 nmol/L). This significant difference between J533 and J415 or J591 also suggests the very high specificity of J415 and J591 mAbs to the $PSMA_{ext}$.

One of the most striking differences among these mAbs was the rate of blood clearance (Fig. 5). On the basis of monoexponential clearance of blood time–activity curves, the rate of blood clearance of ^{131}I-labeled J415 (half-life [$T_{1/2}$] = 3.7 d) and J591 ($T_{1/2}$ = 4.2 d) is somewhat similar and significantly faster than that of 7E11 mAb ($T_{1/2}$ = 7.1 d). With ^{111}In, the half-lives for J415, J591, and 7E11 were 3.4, 2.3, and 5.0 d, respectively.

Compared with ^{131}I labeled antibodies, the tumor uptake of all three ^{111}In-labeled antibodies (J415, J591, and 7E11) gradually increased with time and was quite similar. This finding is also consistent with our previous results (*19*), based on in vitro cellular retention of ^{131}I- and ^{111}In-labeled anti-PSMA mAbs. We have reported that after intracellular binding of either ^{131}I-J415 or ^{131}I-J591, the free ^{131}I was released as I^- from LNCaP cells with half-lives of 31 and

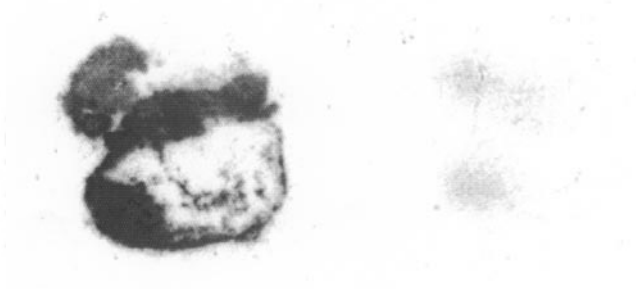

FIGURE 4. Ex vivo autoradiograph of LNCaP tumor section after in vitro incubation with ^{131}I-J591. Autoradiograph on right shows inhibition of ^{131}I-J591 binding in presence of excess cold J591.

38 h, respectively. By contrast, most of the ^{111}In activity was not released from the tumor cell but was trapped within the cell. Because blood clearance of ^{111}In-labeled J415 and J591 is relatively faster than that of 7E11, the tumor-to-blood ratios were 1.5-fold higher at day 6 with J415 and J591, compared with that with 7E11 (Fig. 1B).

The results obtained with ^{111}In-DTPA-7E11 in the LNCaP tumor model at 4 d after injection in our studies (Table 3) were similar to those reported earlier (*23*). Our data are within 20%–30% of the previously reported data (blood: 5.7 ± 0.5 vs. 4.3 ± 0.3; liver: 4.4 ± 0.2 vs. 3.6 ± 0.3; spleen: 3.9 ± 0.8 vs. 2.6 ± 0.3; and tumor: 16.2 ± 2.1 vs. 16.7 ± 1.3). The organ that was significantly different was the kidney (3.8 ± 1.0 vs. 6.7 ± 0.7). They also reported different tumor uptake kinetics showing maximal uptake at 3 d, whereas we observed a gradual increase of uptake up to 6 d. In addition, they showed a wide variation in tumor uptake with different radiolabeled preparations of 7E11 with differing specific activities. For example, on day 3, the tumor uptake was 30 %ID/g for 55.5 kBq/μg and 16.7 %ID/g for 210.9 kBq/μg. In our studies for this report, we evaluated the tumor uptake of ^{131}I- and ^{111}In-labeled mAbs at a specific activity of 148–222 kBq/μg.

Given the finding that 7E11 does not bind viable cells (*23*,*24*), it is interesting to note that the tumor uptake of ^{111}In-labeled 7E11 was similar to that of J415 and J591. We had expected to see a substantial difference in tumor localization based on in vitro studies. The tissue sections and autoradiography, however, provided the explanation. H and E staining showed that, typically, half the tumor mass was necrotic. Given the intracellular location of the 7E11 epitope, it is dead or dying cells that have been postulated to account for tumor localization of 7E11 (*23*,*24*). This indeed was seen, with preferential localization of 7E11 to areas of necrosis (Fig. 3A). mAbs to $PSMA_{ext}$ had a reciprocal pattern to 7E11, with localization concentrated in areas of viable tumor (Fig. 3B). Inability of 7E11 to target well vascularized, viable tumor sites probably explains the inability of ProstaScint to image bone metastases as well as its failure in radioimmunotherapy trials (*21*). mAbs to $PSMA_{ext}$, by targeting viable tumor, should have a better therapeutic effect. In addition, their ability to target viable tumor imparts a better ability to localize well-vascularized sites in the bone marrow (P.M. Smith-Jones et al., unpublished data, 2002).

We have reported that PSMA–antibody complexes are internalized (*18*). Therefore, antibodies such as J415 and J591 may be ideal mAbs for the development of novel therapeutic methods to target the delivery of β- and α-emitting radionuclides for the treatment of tumors expressing PSMA.

The in vitro and in vivo studies with radiolabeled mAbs J415 and J591 clearly demonstrated that these antibodies are highly specific to $PSMA_{ext.}$ Because of in vivo dehalogenation, ^{131}I-labeled mAbs may be inappropriate as a radiolabel with internalizing antibodies. However, ^{111}In-labeled antibodies using the macrocyclic chelating agent DOTA have a highly specific tumor uptake and retention, with optimal tumor-to-blood ratios. Although ^{111}In is not an ideal radionuclide for therapeutic studies, ^{111}In has been well established to be both a chemical and a biologic surrogate for radiometals such as ^{90}Y, ^{177}Lu, and ^{166}Ho. ^{90}Y and several lanthanides (e.g., ^{177}Lu and ^{166}Ho) have been shown to form highly stable complexes with DOTA, similarly to ^{111}In (*25*–*27*). This similarity in chelate chemistry, however, is not applicable for open chelates such as DTPA.

It has been well documented that the radiation dosimetry for ^{90}Y-labeled mAbs and peptides can be estimated on the basis of the pharmacokinetics and biodistribution of the corresponding ^{111}In-labeled mAb analogs (*28*,*29*). Therefore, the biodistribution and tumor localization data with ^{111}In-DOTA-J415 and ^{111}In-DOTA-J591 described in this article support the development of therapeutic radiopharmaceuticals using ^{90}Y (maximum $\beta^- = 2.28$ MeV; $T_{1/2} = 2.67$ d), ^{177}Lu (maximum $\beta^- = 0.497$ MeV; $T_{1/2} = 6.74$ d), and ^{166}Ho (maximum $\beta^- = 1.84$ MeV; $T_{1/2} = 1.12$ d). For most radioimmunotherapeutic agents, the critical organ is the red marrow (*30*). In turn, the marrow radiation dose is determined mainly by the blood radioactivity unless there is specific binding of radiolabeled antibody to bone marrow. In the absence of specific bone marrow localization of the radiopharmaceutical, the therapeutic index (tumor-to-marrow dose) will depend on the kinetics of blood clearance and tumor retention and on the equilibrium dose constant of the radionuclide. With ^{111}In-DOTA-J591, the rate of blood clearance (2.3 d) is faster than the longer retention time of ^{111}In activity within the tumor (^{111}In is essentially trapped within the tumor). As a result, the longer-lived radionuclide, ^{177}Lu, will have greater residence times in tumor than will ^{90}Y. The actual radiation dose (cGy/MBq) to the tumor and marrow will also depend on the β-particle energy. Although it is difficult to predict the therapeutic index for human subjects on the basis of preclinical studies in nude mice, ^{111}In-DOTA-J591 biodistribution studies in nude mice justify preclinical radioimmunotherapeutic studies with ^{90}Y and ^{177}Lu radionuclides. In nude mice bearing LNCaP tumors, we have recently shown a significant antitumor response with both ^{90}Y-DOTA-J591 and ^{177}Lu-DOTA-J591 (*12*,*31*).

CONCLUSION

This article reports the biodistribution and tumor localization of ^{131}I- and ^{111}In-labeled mAbs (J591, J415, and J533) specific to $PSMA_{ext}$. In nude mice bearing PSMA-positive xenografts, the tumor localization of these antibodies was compared with that of radiolabeled 7E11 specific to $PSMA_{int}$. The most important findings were that the blood clearance of ^{111}In-labeled J415 and J591 was relatively faster than that of 7E11, leading to higher tumor-to-blood ratios, compared with that with 7E11. Autoradiographic studies suggest that 7E11 distinctly favors localization to

areas of necrosis whereas J415 and J591 demonstrate a distinct preferential accumulation in areas of viable tumor. These results clearly demonstrate that PSMA-specific internalizing antibodies such as J415 and J591 may be the ideal mAbs for the development of novel therapeutic methods to target the delivery of β-emitting radionuclides (^{131}I, ^{90}Y, and ^{177}Lu) for the treatment of PSMA-positive tumors.

ACKNOWLEDGMENTS

This work was supported by grants from the U.S. Department of the Army (DAMD17-98-1-8594), CaP CURE, and the Yablans Research Fund and the Gerschel Research Fund of the Division of Nuclear Medicine of Weill Medical College of Cornell University.

REFERENCES

1. Murphy GP, Elgamal AA, Su SL, Bostwick DG, Holmes EH. Current evaluation of the tissue localization and diagnostic utility of prostate specific membrane antigen. *Cancer.* 1998;83:2259–2269.
2. Sweat SD, Pacelli A, Murphy GP, Bostwick DG. Prostate-specific membrane antigen expression is greatest in prostate adenocarcinoma and lymph node metastases. *Urology.* 1998;52:637–640.
3. Silver DA, Pellicer I, Fair WR, Heston WDW, Cordon-Cardo C. Prostate specific membrane antigen expression in normal and malignant human tissues. *Clin Cancer Res.* 1997;3:81–85.
4. Troyer JK, Beckett ML, Wright GL Jr. Detection and characterization of the prostate-specific membrane antigen (PSMA) in tissue extracts and body fluids. *Int J Cancer.* 1995;62:552–558.
5. Israeli RS, Powell CT, Corr JG, Fair WR, Heston WDW. Expression of the prostate-specific membrane antigen. *Cancer Res.* 1994;54:1807–1811.
6. Wright GL, Grob BM, Haley C, et al. Up-regulation of prostate specific membrane antigen after androgen-deprivation therapy. *Urology.* 1996;48:326–334.
7. Liu H, Moy P, Kim S, et al. Monoclonal antibodies to the extracellular domain of prostate specific membrane antigen also react with tumor vascular endothelium. *Cancer Res.* 1997;57:3629–3634.
8. Chang SS, Reuter VE, Heston WD, Bander NH, Grauer LS, Gaudin PB. Five different anti-prostate-specific membrane antigen (PSMA) antibodies confirm PSMA expression in tumor-associated neovasculature. *Cancer Res.* 1999;59: 3192–3198.
9. Chang SS, O'Keefe DS, Bacich DJ, Reuter VE, Heston WDW, Gaudin PB. Prostate specific membrane antigen is produced in tumor-associated neovasculature. *Clin Cancer Res.* 1999;5:2674–2681.
10. Dumas F, Gala JL, Berteau F, et al. Molecular expression of PSMA mRNA and protein in primary renal tumors. *Int J Cancer.* 1999;80:799–803.
11. Gregorakis AK, Holmes EH, Murphy GP. Prostate-specific membrane antigen: current and future utility. *Semin Urol Oncol.* 1998;16:2–12.
12. Smith-Jones PM, Vallabhajosula S, Navarro V, Goldsmith SJ, Bander NH. ^{90}Y-huJ591 MAb specific to PSMA: radioimmunotherapy (RIT) studies in nude mice with prostate cancer LNCaP tumor [abstract]. *Eur J Nucl Med.* 2000;8:951.
13. Holmes EH. PSMA specific antibodies and their diagnostic and therapeutic use. *Exp Opin Invest Drugs.* 2001;10:511–519.
14. Horoszewicz JS, Kawinski E, Murphy GP. Monoclonal antibodies to a new antigenic marker in epithelial prostatic cells and serum of prostatic cancer patients. *Anticancer Res.* 1987;7:927–936.
15. Troyer JK, Feng Q, Beckett ML, Wright GL Jr. Biochemical characterization and mapping of the 7E11–C5.3 epitope of the prostate-specific membrane antigen. *Urol Oncol.* 1995;1:29–37.
16. Kahn D, Williams RD, Seldin DW, et al. Radioimmunoscintigraphy with ^{111}indium labeled CYT-356 for the detection of occult prostate cancer recurrence. *J Urol.* 1994;152:1490–1495.
17. Petronis JD, Regan F, Lin K. Indium-111 capromab pendetide (ProstaScint) imaging to detect recurrent and metastatic prostate cancer. *Clin Nucl Med.* 1998;23:672–677.
18. Liu H, Rajasekaran AK, Moy P, et al. Constitutive and antibody-induced internalization of prostate specific membrane antigen. *Cancer Res.* 1998;58:4055–4060.
19. Smith-Jones PM, Vallabahajosula S, Goldsmith SJ, et al. In vitro characterization of radiolabeled monoclonal antibodies specific for the extracellular domain of prostate specific membrane antigen. *Cancer Res.* 2000;60:5237–5243.
20. Fraker PJ, Speck JC. Protein and cell membrane iodinations with a sparingly soluble chloramide, 1,3,4,6-tetrachloro-3a,6a-diphenylglycoluril. *Biochem Biophys Res Commun.* 1978;80:849–857.
21. Deb N, Goris M, Trisler K, et al. Treatment of hormone-refractory prostate cancer with ^{90}Y-CYT-356 monoclonal antibody. *Clin Cancer Res.* 1996;2:1289–1297.
22. Lindmo T, Boven E, Cuttitta F, Fedorko J, Bunn PA. Determination of the immunoreactive fraction of radiolabeled monoclonal antibodies by linear extrapolation to binding at infinite antigen excess. *J Immunol Methods.* 1994;72:77–89.
23. Lopes AD, Davis WL, Rosenstraus MJ, Uveges AJ, Gilman SC. Immunohistochemical and pharmacokinetic characterization of the site-specific immunoconjugate CYT-356 derived from antiprostate monoclonal antibody 7E11–C5. *Cancer Res.* 1990;50:6423–6429.
24. Troyer JK, Beckett ML, Wright GL Jr. Location of prostate-specific membrane antigen in the LNCaP prostate carcinoma cell line. *Prostate.* 1997;30:232–242.
25. Locin MF, Desreux JF, Merciny E. Coordination of lanthanides by two polyamino polycarboxylic macrocycles: formation of highly stable lanthanide complexes. *Inorg Chem.* 1986;25:2646–2648.
26. Clarke ET, Martel AE. Stabilities of trivalent metal ion complexes of the tetraacetate derivatives of 12-, 13- and 14-membered tertaazamacrocycles. *Inorganica Chimica Acta.* 1991;190:37–46.
27. Broan CJ, Cox JPL, Craig AS, et al. Structure and solution stability of indium and gallium complexes of 1,4,7-triazacyclononanetriacetate and of yttrium complexes of 1,4,7,10-tetraazacyclododecanetetraacetate and related ligands: kinetically stable complexes for use in imaging and radiotherapy—x-ray molecular structure of the indium and gallium complexes of 1,4,7-triazacyclononane-1,4,7-triacetic acid. *J Chem Soc Perkin Trans II.* 1991;2:87–99.
28. DeNardo SJ, Kramer EL, O'Donnell RT, et al. Radioimmunotherapy for breast cancer using indium-111/yttrium-90 BrE-3: results of a phase I clinical trial. *J Nucl Med.* 1997;38:1180–1185.
29. Carrasquillo JA, et al. Similarities and differences in ^{111}In- and ^{90}Y-labeled 1B4M-DTPA anti-tac monoclonal antibody distribution. *J Nucl Med.* 1999;40: 268–276.
30. Behr TM, Sgouros G, Vougioukas V, et al. Therapeutic efficacy and dose-limiting toxicity of Auger-electron vs. beta emitters in radioimmunotherapy with internalizing antibodies: evaluation of ^{125}I- vs. ^{131}I-labeled CO17-iA in a human colorectal cancer model. *Int J Cancer.* 1998;76:738–748.
31. Smith-Jones PM, Navarro V, Omer SS, Bander NH, Goldsmith SJ, Vallabhajosula S. Comparative anti-tumor effects of ^{90}Y-DOTA-J591 and ^{177}Lu-DOTA-J591 in nude mice bearing LNCaP tumors [abstract]. *J Nucl Med.* 2001;42(suppl): 151P–152P.